Coherent quantum transport in the presence of a finite-range transversely polarized time-dependent field

C.S. Tang[a], C.S. Chu[b],*

[a]*Department of Electronic Engineering, Tung Nan Junior College of Technology, Taipei 22202, Taiwan, ROC*
[b]*Department of Electrophysics, National Chiao Tung University, Ta Hsueh Road, Hsinchu 30010, Taiwan, ROC*

Abstract

This work investigates the quantum transport in a narrow constriction acted upon by a finite-range transversely polarized time-dependent field. A generalized scattering-matrix method is developed that has incorporated a time-dependent mode-matching scheme. The transverse field induces coherent inelastic scatterings that include both intersubband and intersideband transitions. These scatterings give rise to the DC conductance G a general suppressed feature that escalates with the chemical potential. In addition, particular suppressed features – the dip structures – are found in G. These features are recognized as the quasibound state (QBS) features that arise from electrons making intersubband transitions to the vicinity of a subband bottom. For the case of larger field intensities, the QBS features that involve more photons are more evident. These QBS features are closely associated with the singular density of states at the subband threshold. An experimental setup is proposed for the observation of these features. © 2000 Elsevier Science B.V. All rights reserved.

Keywords: Coherent quantum transport; Narrow constriction; Quasibound state; Time-dependent field

1. Introduction

Advances in the epitaxial growth technologies have lead to the fabrication of high-quality two-dimensional electron gas (2DEG) systems that are almost defect-free and upon which electronic nanostructures can be built. The electron transport properties of these nanostructures have been extensively studied and by now many aspects are well understood [1,2]. The most studied structure is the quantum point contact (QPC), due to its simple configuration, and also due to the significant quantization effects in such systems, as is shown in the conductance G [3,4].

These QPCs, when created electrostatically by negatively biasing a split-gate located on top of a 2DEG [3,4], can be pictured as a narrow constriction connecting adiabatically at each end to a 2DEG [5,6], as depicted in Fig. 1. The energy levels in the narrow constriction are quantized into one-dimensional subbands which density of states (DOS) is singular just below the subband threshold. This singular DOS was found, in the presence of an attractive scatterer, to give rise to dip structures in G, which is associated with the formation of

* Corresponding author. Tel.: + 886-3-5712121 ext. 56127; fax: + 886-3-5725230.

E-mail addresses: cstang@cc.nctu.edu.tw (C.S. Tang), cschu@cc.nctu.edu.tw (C.S. Chu).
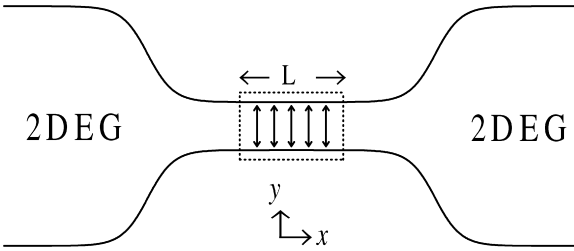
Fig. 1. Sketch of the gated QPC which is connected at each end to a two-dimensional electron gas electrode. The narrow constriction is acted upon by a transversely polarized time-dependent electric field within millimeter wave region.

impurity-induced quasibound states (QBSs) [7–9] formed just below the subband threshold.

More recently, attentions have been shifted to QPCs acted upon by high-frequency fields. These fields include transversely [10–22], or longitudinally [23,24] polarized fields, or simply gate-induced time-modulated potentials [25–27]. These studies focus on coherent inelastic scatterings by assuming the range of the time-modulation to be shorter than the incoherent mean free path. A number of interesting transport characteristics were explored. First, the mechanisms of photovoltaic effect subject to an unbiased asymmetric QPC was proposed [10]. Second, photon-associated transport phenomena in QPCs have been studied [11–20]. Third, current noise in an irradiated QPC has also been studied [28]. However, the QBS features induced by such high-frequency field are not widely recognized.

Our previous work has investigated electron transport characteristics subject to a longitudinally polarized time-dependent field [24]. This longitudinal field is uniform in the *y* direction such that the mode-matching method is valid. This matching scheme allows detail analysis of the transport characteristics. However, as long as the field is transversely polarized, this scheme is unstable when the photon sideband energy is approximately equal to the subband energy-level spacing, not shown here. Hence, one has to develop other method to calculate the effects of such transverse field on the photoconductance *G* through a mesoscopic nanostructure.

In theoretical studies of quantum transport in mesoscopic systems, both the transfer-matrix and

the scattering-matrix method are powerful tools. The two methods enable us to numerically calculate current transmission coefficients for arbitrary time-modulated profile or confinement potential. The former method, however, is unstable for higher field amplitudes or longer time-modulated range. Thus, as we show later, the latter method is used to numerically calculate the current transmission coefficients. The conductance of the nanostructure can then be obtained similar to the Landauer–Büttiker formalism [29].

In this paper, we develop a generalized scattering-matrix method for numerical calculation of *G* in mesoscopic systems, that are applied by an AC signal without AC bias between the reservoirs. Specifically, we focus on the situation that a transversely polarized time-dependent field acts upon the narrow constriction, as depicted in Fig. 1. This localized field breaks the longitudinal translational invariance of the electron motion, and hence allows electrons to make *intersideband* transitions not to conserve their longitudinal momenta [21,26]. Moreover, since the applied field is not uniform in the *y* direction, the transverse translational invariance is also violated. Thus the electron–photon scattering processes can make *intersubband* transitions. These mixed transitions are quite different with our previous works [24,26] and make the analytical formulation and numerical calculation complicated.

This paper is organized as follows. In Section 2, the generalized scattering-matrix method is developed that has incorporated a time-dependent mode-matching scheme to solve the time-dependent Schrödinger equation. The method described in Section 2 is calculated numerically in Section 3. From our numerical examples, we conclude that QBS features can occur when a transversely polarized field acts upon the narrow constriction. Concluding remarks are given in Section 4.

2. Theory

In this section, we establish a generalized scattering-matrix method to study the electron transport properties in narrow constrictions which is acted upon by a transversely polarized time-dependent

field. This field is sliced into a series of strips. By performing the time-dependent mode-matching between these strips in the cascading of the scattering matrices, we obtain the transmission and reflection coefficients. The conductance G is then expressed in terms of these coefficients.

Since the field is assumed to be localized, we need only to formulate this time-modulated scattering problem in the narrow constriction region. We consider the ballistic regime such that the typical dimension of the constriction is smaller than the phase-breaking length. In addition, to simplify the calculation, we neglect the electron–electron interaction in the constriction. Thus, the electron transport can be described by a time-dependent Schrödinger equation with Hamiltonian of the form

$$\mathscr{H}(\boldsymbol{x},t) = \left[\boldsymbol{p} + \frac{e}{c} \boldsymbol{A}(\boldsymbol{x},t) \right]^2 + V_c(y). \qquad (1)$$

Here $\boldsymbol{p}$ represents the momentum of an electron and $V_c(y)$ denotes the transverse confinement of the narrow constriction modeled by a quadratic potential [30]. We consider the field has a finite longitudinal profile $\boldsymbol{E}(\boldsymbol{x},t) = \mathscr{E}(x)\cos(\omega t)\hat{y}$, namely that $\mathscr{E}(x)$ does not act on the two-end electrodes of the constriction between which the bias is applied. Taking the Coulomb gauge, the effect of the applied field can be represented by a vector potential

$$\boldsymbol{A}(\boldsymbol{x},t) = -\frac{c}{\omega} \mathscr{E}(x)\sin(\omega t)\hat{y}, \qquad (2)$$

where $\mathscr{E}(x)$ represents the profile of the field with amplitude $\mathscr{E}_0$ for $|x| < L/2$ and vanishes otherwise. Here we would like to bring the attention that the Gaussian profile has also been adopted instead of the simplified abrupt profile, not shown here. However, the two profiles lead to similar features in G. Thus, the results in the abrupt profile approximation should be qualitatively sound.

Below we choose the length unit $a^* = 1/k_F$, the energy unit $E^* = \hbar^2 k_F^2/(2m^*)$, the time unit $t^* = \hbar/E^*$, and field amplitude $\mathscr{E}_0$ in units of $E^*/(ea^*)$, where $-e$ denotes the electron charge, with effective mass m^*, and k_F represents the magnitude of a typical Fermi wave vector of the reservoir. Thus, we can write the dimensionless transverse confine-

ment $V_c(y) = \omega_y^2 y^2$, and then gives the quantized transverse energy levels $\varepsilon_n = (2n+1)\omega_y$ and the corresponding wave function $\phi_n(y)$.

We slice the field into N_L strips, denote the width of every strip as $\delta L = L/N_L$, and ensure δL is sufficiently narrow such that every strip can be described by a delta-profile. These strips are located at $x_i = -L/2 + (i-1/2)\delta L$, where $i = 1, 2, \ldots, N_L$. The effective Schrödinger equation of the ith strip is then given by

$$i\frac{\partial}{\partial t} \Phi^{(i)}(\boldsymbol{x},t) = \left[-\left(\frac{\partial^2}{\partial x^2} + \frac{\partial^2}{\partial y^2} \right) + \omega_y^2 y^2 \right.$$
$$+ \left(i\frac{2\mathscr{E}_0}{\omega}\frac{\partial}{\partial y}\sin(\omega t) + \frac{\mathscr{E}_0^2}{\omega^2}\sin^2(\omega t) \right)$$
$$\left. \times \delta L \delta(x - x_i) \right] \Phi^{(i)}(\boldsymbol{x},t). \qquad (3)$$

Consider an electron, in the nth subband and with kinetic energy μ', incident from the left-hand side of the ith strip, one can write the scattering wave function [21]

$$\Phi_n^{(i)}(\boldsymbol{x},t) = \phi_n(y)\exp[ik_n(\mu')x - i\mu't]$$
$$+ \sum_{n',m'} r_{n'n}^{(i)}(m')\phi_{n'}(y)\exp[-ik_{n'}(\mu'+m'\omega)x]$$
$$\times \exp[-i(\mu'+m'\omega)t] \quad \text{if } x < x_i, \qquad (4)$$

$$\Phi_n^{(i)}(\boldsymbol{x},t) = \sum_{n',m'} t_{n'n}^{(i)}(m')\phi_{n'}(y)\exp[ik_{n'}(\mu'+m'\omega)x]$$
$$\times \exp[-i(\mu'+m'\omega)t] \quad \text{if } x > x_i, \qquad (5)$$

where the electron is scattered into the intermediate subband n' and sideband m'. Here $k_n(\mu') = \sqrt{\mu' - \varepsilon_n}$ represents the magnitude of wave vector for the nth subband electron with kinetic energy μ'. The effective wave function of the ith strip is then given by $\Phi^{(i)}(\boldsymbol{x},t) = \sum_n \Phi_n^{(i)}(\boldsymbol{x},t)$. The boundary conditions of these strips are given by

$$\Phi_n^{(i)}|_{x = x_i - \delta} = \Phi_n^{(i)}|_{x = x_i + \delta} \qquad (6)$$

and

$$\frac{\partial \Phi_n^{(i)}}{\partial x}\bigg|_{x = x_i + \delta} - \frac{\partial \Phi_n^{(i)}}{\partial x}\bigg|_{x = x_i - \delta} = \left[i\frac{2\mathscr{E}_0}{\omega}\frac{\partial}{\partial y}\sin(\omega t) \right.$$
$$\left. + \frac{\mathscr{E}_0^2}{\omega^2}\sin^2(\omega t) \right] \delta L \Phi_n^{(i)}(x = x_i). \qquad (7)$$

Imposing the boundary conditions (6) and (7) to perform the matching at all times and given the expression of the matrix element

$$\left\langle l \left| \frac{\partial}{\partial y} \right| n' \right\rangle = \sqrt{\frac{\omega_y}{2}} [\sqrt{'} \delta_{l,n'-1} - \sqrt{n'+1} \delta_{l,n'+1}], \quad (8)$$

we obtain the equations relating the reflection coefficients $r_{ln}^{(i)}(m)$ and the transmission coefficients $t_{ln}^{(i)}(m)$,

$$t_{ln}^{(i)}(m) - r_{ln}^{(i)}(m) = \delta_{m,0} \delta_{n,l} \quad (9)$$

and

$$\delta_{m,0} \delta_{n,l} k_n(\mu') = k_l(\mu' + m\omega)[r_{ln}^{(i)}(m) + t_{ln}^{(i)}(m)]$$
$$+ i \frac{\mathscr{E}_0}{\omega} \delta L \sum_{n',m'} [\delta_{m',m+1} - \delta_{m',m-1}] \left\langle l \left| \frac{\partial}{\partial y} \right| n' \right\rangle t_{n'n}^{(i)}(m')$$
$$+ i \frac{\mathscr{E}_0^2}{4\omega^2} \delta L [2t_{ln}^{(i)}(m) + t_{ln}^{(i)}(m+2) + t_{ln}^{(i)}(m-2)].$$
$$(10)$$

From these expressions, it turns out that the electrons do not conserve their longitudinal momenta. This means when the time-dependent field has a local profile, the possibility of these transition processes can be made. In Eq. (10), we can see that the $\mathscr{E}_0$ terms cause the transitions associated with one-photon processes, while the $\mathscr{E}_0^2$ terms contribute to two-photon processes. By solving Eqs. (9) and (10), we obtain the transmission coefficients $t_{ln}^{(i)}(m)$ and reflection coefficients $r_{ln}^{(i)}(m)$ of the ith strip. For an electron incident from the right-hand side of the ith strip, the transmission coefficient $\tilde{t}_{ln}^{(i)}(m)$ and the reflection coefficient $\tilde{r}_{ln}^{(i)}(m)$ differ from those from the left-hand side of the ith strip only by a phase factor of unit modulus, given by

$$\tilde{t}_{ln}^{(i)}(m) = t_{ln}^{(i)}(m) \exp\{2i[k_l(\mu' + m\omega) - k_n(\mu')]x_i\} \quad (11)$$

and

$$\tilde{r}_{ln}^{(i)}(m) = r_{ln}^{(i)}(m) \exp\{-2i[k_l(\mu' + m\omega) + k_n(\mu')]x_i\}. \quad (12)$$

Generally, for an electron incident from the left-hand side of the ith strip in the subband n_{i-1} and at energy $\mu + m_{i-1}\omega$, this state is denoted as $\alpha_{i-1} = (n_{i-1}, m_{i-1})$. The electron may be transmitted into the state $\alpha_i = (n_i, m_i)$ with a transmission

coefficient $t_{\alpha_i,\alpha_{i-1}}$, or reflected into the state β_{i-1} with a reflection coefficient $r_{\beta_{i-1},\alpha_{i-1}}$. Similarly, for an electron incident from the right-hand side of the ith strip in the state β_i, the corresponding transmission and reflection coefficient are given by $\tilde{t}_{\beta_{i-1},\beta_i}$ and $\tilde{r}_{\beta_{i-1},\beta_i}$, respectively. After defining these coefficients, we can establish the scattering-matrix equation, given by

$$\begin{bmatrix} A_i \\ B_{i-1} \end{bmatrix} = S(i-1,i) \begin{bmatrix} A_{i-1} \\ B_i \end{bmatrix}, \quad (13)$$

where A_i and B_i are the coefficients of the right- and the left-going states in the ith region, respectively, as illustrated in Fig. 2. Here $S(i-1,i)$ is the scattering matrix which connects between the $(i-1)$th and the ith region, given by

$$S(i-1,i) = \begin{bmatrix} t(i) & \tilde{r}(i) \\ r(i) & \tilde{t}(i) \end{bmatrix}. \quad (14)$$

Here, $t(i)$ and $r(i)$ denote the transmission and reflection matrices of the right-going electron at the ith strip, respectively, and the tilded two refer to the contribution of left-going electron. Matching between these strips has to be performed in the cascading of the scattering matrices. We would like to point out the reason for using the scattering-matrix formalism, instead of the transfer-matrix method, is to avoid the use of truncation schemes required in dealing with the exponentially growing solutions [31].
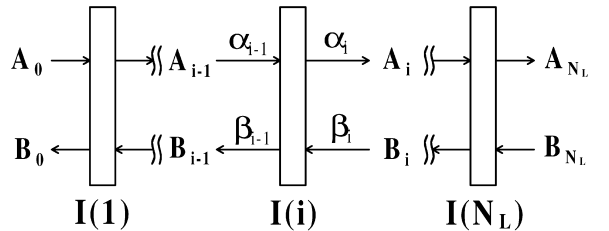

Fig. 2. Sketch of the time-dependent field, which is sliced into N_L strips. The coefficients of the right- and left-going states of the ith region are denoted as A_i and B_i, respectively. These coefficients between successive regions are connected by the interface matrix $I(i)$. The α_i and β_i represent dummy indices of the ith region, including both subband and sideband indices.

Start from rearranging Eq. (13), we obtain the matrix equation

$$\begin{bmatrix} A_{i-1} \\ B_{i-1} \end{bmatrix} = I(i) \begin{bmatrix} A_i \\ B_i \end{bmatrix}, \qquad (15)$$

which connects the coefficients of the successive regions across the ith strip. Here $I(i)$ represents the interface matrix of the ith strip, defined by

$$I(i) = \begin{bmatrix} I_{11}(i) & I_{12}(i) \\ I_{21}(i) & I_{22}(i) \end{bmatrix}, \qquad (16)$$

in which

$$I_{11}(i) = t(i)^{-1},$$

$$I_{12}(i) = -t(i)^{-1}\tilde{r}(i),$$

$$I_{21}(i) = r(i)t(i)^{-1},$$

$$I_{22}(i) = \tilde{t}(i) - r(i)t(i)^{-1}\tilde{r}(i). \qquad (17)$$

Generally, for the regions up to the $(i-1)$th strip, we have

$$\begin{bmatrix} A_{i-1} \\ B_0 \end{bmatrix} = S(0, i-1) \begin{bmatrix} A_0 \\ B_{i-1} \end{bmatrix}, \qquad (18)$$

where $S(0, i-1)$ represents the scattering matrix connecting the 0th region to the $(i-1)$th region, defined by

$$S(0, i-1) = \begin{bmatrix} S_{11}(0, i-1) & S_{12}(0, i-1) \\ S_{21}(0, i-1) & S_{22}(0, i-1) \end{bmatrix}. \qquad (19)$$

Imposing Eqs. (15) and (18), the coefficients A_{i-1} and B_{i-1} may be eliminated, and then we obtain the matrix equation connecting the 0th to the ith region, given by

$$\begin{bmatrix} A_i \\ B_0 \end{bmatrix} = S(0, i) \begin{bmatrix} A_0 \\ B_i \end{bmatrix}. \qquad (20)$$

The submatrices of $S(0, i)$ are, explicitly,

$$S_{11}(0, i) = [I_{11}(i) - S_{12}(0, i-1)I_{21}(i)]^{-1}$$
$$\times S_{11}(0, i-1),$$

$$S_{12}(0, i) = [I_{11}(i) - S_{12}(0, i-1)I_{21}(i)]^{-1}$$
$$\times [S_{12}(0, i-1)I_{22}(i) - I_{12}(i)],$$

$$S_{21}(0, i) = S_{21}(0, i-1) + S_{22}(0, i-1)I_{21}(i)S_{11}(0, i),$$

$$S_{22}(0, i) = S_{22}(0, i-1)I_{22}(i) + S_{22}(0, i-1)$$
$$\times I_{21}(i)S_{12}(0, i). \qquad (21)$$

This iterative procedure is not as easy to evaluate in terms of the transfer-matrix method, which simply inverses a product of matrices. More precisely, once the system is acted upon by an external time-modulated field, the evanescent modes play an important role due to inelastic scatterings. We prefer to use the scattering-matrix method to gain the stability for the numerical computation. By iterating Eq. (21), we obtain the scattering matrix $S(0, N_L)$ which satisfies the matrix equation

$$\begin{bmatrix} A_{N_L} \\ B_0 \end{bmatrix} = S(0, N_L) \begin{bmatrix} A_0 \\ B_{N_L} \end{bmatrix}. \qquad (22)$$

This equation describes the electron transport through the whole time-modulated region. The incident state is $\alpha_{in} = (n_0, 0)$ such that the elements of the incident coefficient A_0 can be expressed as $\delta_{n,n_0}\delta_{m,0}$. Setting $B_{N_L} = 0$, we have $A_{N_L} = S_{11}(0, N_L)A_0$ and $B_0 = S_{21}(0, N_L)A_0$.

For an electron incident from the initial state $\alpha_{in} = (n_0, 0)$ and transmitted into the final state $\alpha_f = (n_f, m_f)$, whose transmission coefficient is denoted by $t_{\alpha_f, \alpha_{in}} = (A_{N_L})_{\alpha_f}$ – an element of A_{N_L}. The current transmission coefficient, corresponding to this inelastic scattering process, is then given by

$$T_{\alpha_{in}}^{\alpha_f} = \left[\frac{k_{n_f}(\mu + m_f\omega)}{k_{n_0}(\mu)} \right] |t_{\alpha_f, \alpha_{in}}|^2. \qquad (23)$$

The zero-temperature conductance can then be obtained, given by

$$G = \frac{2e^2}{h} \sum_{\alpha_{in}} \sum_{\alpha_f} T_{\alpha_{in}}^{\alpha_f} = \frac{2e^2}{h} \sum_{\alpha_{in}} T_{\alpha_{in}}, \qquad (24)$$

where $T_{\alpha_{in}}$ represents the current transmission coefficient from the incident state α_{in}. Here the summation $\sum_{\alpha_{in}} = \sum_{n_0=0}^{N}$, and $N+1$ denotes the number of propagating subbands for the chemical potential μ. For the final states, $\sum_{\alpha_f} = \sum_{n_f=0}^{N} \sum_{m_f}'$ is expected to be a double sum. Here the superscript prime indicates that summation is over m_f such that $k_{n_f}(\mu + m_f\omega)$ is real, namely that only occupied subbands are included. The conservation of

current, given by the condition

$$\sum_{\alpha_f} \frac{k_{n_f}(\mu + m_f\omega)}{k_{n_0}(\mu)}[|t_{\alpha_f,\alpha_{in}}|^2 + |r_{\alpha_f,\alpha_{in}}|^2] = 1 \qquad (25)$$

is used to check our numerical accuracy.

3. Numerical results and discussion

In this section, the characteristics of the conductance G are studied. We have shown in our previous work that conductance behavior is insensitive to L except for the harmonic structures [24]. Thus, we fix the length L of the time-modulated region while varying the field amplitude $\mathscr{E}_0$. The G characteristics are represented by the dependence on X, the suitably rescaled chemical potential μ, is given by

$$X = \frac{\mu}{\Delta\varepsilon} + \tfrac{1}{2}.$$

With this conversion, the integral value of X represents the number of propagating subbands through the narrow constriction. When μ is changed by a subband energy-level spacing $\Delta\varepsilon$, it corresponds to $\Delta X = 1$; and when μ is changed by $\hbar\omega$, it corresponds to $\Delta X = \omega/\Delta\varepsilon$.

In our numerical examples, the physical parameters are chosen to be that in a high-mobility modulation-doped GaAs–Al$_x$Ga$_{1-x}$As heterostructure with a typical electron density $n \sim 2.5 \times 10^{11}$ cm^{-2}, and $m^* = 0.067$ m$_e$. Correspondingly, we choose a length unit $a^* = 1/k_F = 79.6$ Å, an energy unit $E^* = \hbar^2 k_F^2/(2m^*) = 9$ meV, and an angular frequency unit $\omega^* = E^*/\hbar = 13.6$ Trad/s. We also choose $\omega_y = 0.035$ such that the subband energy-level spacing $\Delta\varepsilon = 0.07$ ($= 0.63$ meV), and the effective narrow constriction width is of the order of 0.1 μm. We also choose the angular frequencies as $\omega = 0.028$ ($v = \omega/2\pi \cong$ 61 GHz) and 0.042 ($v \cong 91$ GHz), for Figs. 3 and 4, respectively. The time-modulated range in both the figures was chosen to be $L = 50$ ($\simeq 0.4$ μm).

In Figs. 3a–c, the field amplitudes are chosen to be $\mathscr{E}_0 = 0.002$, 0.003, and 0.004 for Figs. 3a–c, respectively. The angular frequency $\omega = 0.028$ corresponds to an energy interval $\Delta X = \omega/\Delta\varepsilon = 0.4$
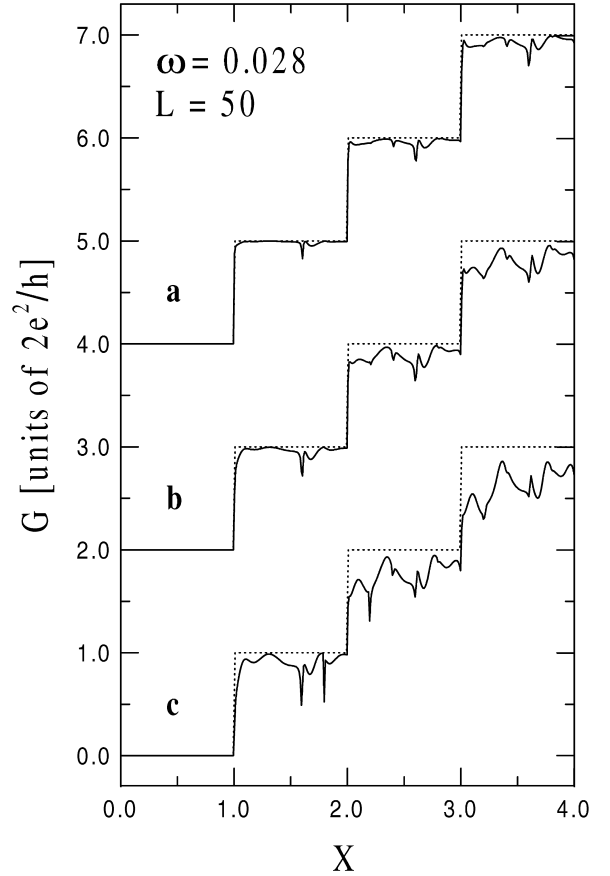

Fig. 3. Conductance G as a function of X for frequency $\omega = 0.028$ ($\simeq 0.4\Delta\varepsilon$), with time-modulated range $L = 50$. The amplitude of the electric field are $\mathscr{E}_0 =$ (a) 0.002 ($\simeq 22.6$ V/cm); (b) 0.003 ($\simeq 33.9$ V/cm); and (c) 0.004 ($\simeq 45.2$ V/cm). The curves are vertically offset for clarity.

for Figs. 3a–c, respectively. The dotted curves are the unperturbed results. Generally, we find the suppressed features in G that escalate with both the chemical potential and $\mathscr{E}_0$, as illustrated in Figs. 3a–c. In addition, there are dip structures in G, which can be understood to be the formation of photo-induced QBSs, where electrons are trapped temporarily due to the singular DOS just below the subband threshold [21,24].

Figs. 3a–c have common types of suppressed structures. First, dip structures are found at around $X = (N + 1) - \Delta X$. These structures are induced by the electrons, incident in the Nth subband with kinetic energy $(N + 1) - \Delta X$, that can absorb ΔX
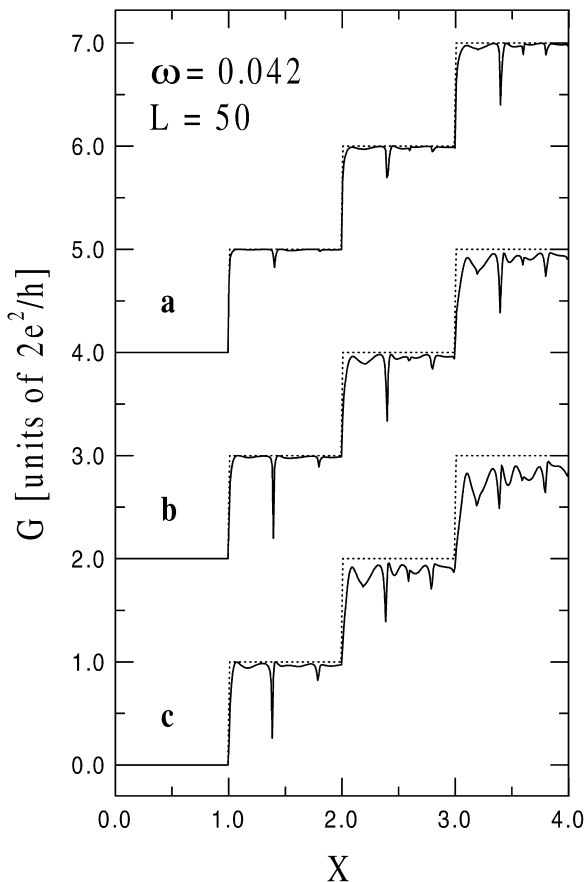
Fig. 4. Conductance G as a function of X for frequency $\omega = 0.042$ ($\simeq 0.6\Delta\varepsilon$), with time-modulated range $L = 50$. The amplitude of the electric field are $\mathscr{E}_0 =$ (a) 0.002 ($\simeq 22.6$ V/cm); (b) 0.003 ($\simeq 33.9$ V/cm); and (c) 0.004 ($\simeq 45.2$ V/cm). The curves are vertically offset for clarity.

to form QBSs just below the $(N + 1)$th subband threshold. These transitions are recognized as $(\Delta n, \Delta m) = (+1, +1)$ processes. Second, small dip structures are found at around $X = N + \Delta X$. These structures are induced by the electrons, incident in the Nth subband with kinetic energy $N + \Delta X$, can emit ΔX to form QBSs just below the $(N + 1)$th subband threshold. These are $(+1, -1)$ transitions. Third and alternatively, dip structures at around $X = 2.2$ and 3.2 are combinations of two different kind of transitions: $(+2, +2)$ and $(-1, -3)$ processes. The former features are induced by the electrons, incident in the Nth subband with kinetic energy $(N + 2) - 2\Delta X$, that can

absorb $2\Delta X$ to the form QBSs just below the $(N + 2)$th subband threshold; while the latter features are induced by the electrons, incident in the Nth subband with kinetic energy $(N - 1) + 3\Delta X$, that can emit $3\Delta X$ to the $(N - 1)$th subband threshold.

Interestingly, in Figs. 3b and c, small dip structures at around $X = N$ are found. These structures are induced by the electrons, incident in the Nth subband with kinetic energy N, that can absorb ΔX to the $(N + 1)$th subband intermediate state and then emit ΔX to the $(N + 2)$th suband final state. These are two-step $(+2, 0)$ intersubband and intrasideband transitions. In addition, in Figs. 3b–c, small dips at around $X = N + 2\Delta X$ are recognized. These structures are induced by the electrons incident in the Nth subband with kinetic energy $N + 2\Delta X$. These electrons can emit ΔX to the $(N + 1)$th subband intermediate state and then emit ΔX to the Nth suband final state. These are two-step $(0, -2)$ intrasubband and intersideband transitions. Since these structures involve two transitions to form QBSs, these are found for higher field intensities. From the above analysis, we conclude that the photo-induced transitions must obey the selection rule $\Delta n + \Delta m = $ even.

In the previous work [24], we have studied the electron transport characteristics when a longitudinally polarized time-dependent field acts upon narrow constrictions. It is shown that an effective potential barrier for height $\Delta X_V = \mathscr{E}_0^2/(2\omega^2\Delta\varepsilon)$ is involved in G due to the A^2 term in the Hamiltonian. This effective potential barrier causes a transmitting Nth subband electron, with incident energy $N \leqslant X < N + \Delta X_V$, to transmit via direct tunneling, or to transmit via assisted transmission by absorbing photon energies. Here we note that for the case of transversely polarized field, this effective potential is not dominant. Hence, there are sharp dip structures instead of valleylike structures. The result may explain that most of the electrons either emit or absorb photons and reach the QBSs that are formed just below the subband threshold *outside* the time-modulated region.

In Fig. 4, the field amplitudes are chosen to be of the same as Fig. 3. The angular frequency $\omega = 0.042$ corresponds to an energy interval $\Delta X = 0.6$. There are common types of dip structures in

Figs. 4a–c. First, sharp dip structures are found at around $X = (N + 1) - \Delta X$. These structures are induced the electron, incident in the Nth subband with kinetic energy $(N + 1) - \Delta X$, can absorb ΔX to form QBS beneath the $(N + 1)$th subband threshold. These structures correspond to $(+ 1, + 1)$ transitions. Second, small dips at around $X = (N + 1) + \Delta X$ are found. These dips are induced by the electron, incident in the Nth subband with kinetic energy $(N + 1) + \Delta X$, can emit ΔX to form QBS beneath the $(N + 1)$th subband threshold. These are $(+1, -1)$ transitions. Since the momentum transfer of the first case in less than the second one so that transition probabilty of $(+ 1, + 1)$ is greater than the $(+ 1, - 1)$ process. Thus the electron trapping ability of the first kind is stronger then the second one. Third, the dips at around $X = (N + 2) - 2\Delta X$ are found. These dips are induced by the electron, incident in the Nth subband with kinetic energy $(N + 2) - 2\Delta X$, can absorb $2\Delta X$ to form QBS beneath the $(N + 2)$th subband threshold. These are $(+ 2, + 2)$ transition processes. Fourth and alternatively, in Figs. 4b and c, dip structures at around $X = N$ are found. These structures can be identified as $(+ 2, 0)$ two-step intersubband and intrasideband transitions. Finally, in Fig. 4c, there are dips at around $X = N + 2\Delta X$, which are associated with $(0, - 2)$ two-step intrasubband and intersideband transitions.

We want to bring attention that to observe the above predicted effects, the experimental setup needs to fulfill two requirements. First, the bolometric heating due to the absorption of photons in the QPCs end-electrodes has to be suppressed or totally eliminated. Recent experiments show that the transport characteristics are masked by the bolometric effect when the entire QPC, including the two-end electrodes, is exposed to the incident electromagnetic field [15]. Second, the time-modulated range has to be shorter than the wave length of the incident field. The purpose is to increase the coupling between the electrons and the photons by breaking the longitudinal-translational invariance. That the coupling between the external field and the conduction electrons can be much enhanced, when either the electrons are confined or the time-dependent field has a localized profile, has been pointed out by Yakubo et al. [32]. Thus the QPC needs to be modulated in the near-field regime.

To avoid the bolometric heating, we suggest to apply AC signal to the split-gates of the QPC instead of shining an electromagnetic wave upon the QPC. The split-gates are negatively biased with respect to a common ground, and made of superconducting materials with superconducting wires connecting to an AC-signal generator. This generator can be available using the IMPATT diode that has successfully been demonstrated to cover the complete millimeter wave range (see for example [33]). This proposed experimental setup is expected to generate a transversely polarized field only in the narrow constriction region while keeping the two-end electrodes from the time-modulation. In the present work, though the time-modulated region covers only part of the narrow constriction, we believe these two situations will manifest similar features. Given the availability of millimeter wave sources [33], we may design the system that make QBS features feasible experimentally with techniques currently available. The features reported in this work, however, are not limited to millimeter wave region.

4. Conclusion

A generalized scattering-matrix method has been developed for investigating quantum transport in narrow constrictions applied by an external time-dependent field. This method, though very time consuming, allows us to solve the time-dependent Schrödinger equation exactly in the numerical sense. Since the energy conservation law is violated in such a time-modulated system, a conventional transfer-matrix method technique is inapplicable. Using the present numerical method, not only the transmission and reflection probabilities of the time-modulated systems can be calculated, all the subband and sideband states can be obtained. We hope that the present method will be utilized to study new transport phenomena in arbitrary time-modulated mesoscopic systems. Numerical efficiency, however, is needed to improve for this extension and also for taking the self-consistent scheme into consideration.

The present results indicate rich behavior in the time-averaged conductance when a loacalized transversely polarized time-dependent field is applied to a QPC in the regime where the photon energy is comparable to the subband energy-level spacing. Dip structures are clearly found in conductance when the constriction is acted upon by such localized field. These dip structures are associated with the electrons that can make both intersubband (or intrasubband) and intersideband (or intrasideband) transitions to form QBSs situated just below the subband threshold. In addition, attributed to the sensitivity of the QBSs to the frequency and intensity of the field, the proposed geometry may function as a useful spectroscopy tool. We hope that our work will inspire experimental investigaion of these phenomena in time-modulated QPC devices.

Acknowledgements

References

[1] D.K. Ferry, S.M. Goodnick, Transport in Nanostructures, Cambridge University Press, Cambridge, UK, 1997.
[2] Y. Imry, Introduction to Mesoscopic Physics, Oxford University Press, Oxford, UK, 1997.
[3] B.J. van Wees, H. van Houton, C.W.J. Beenakker, J.G. Williamson, L.P. Kouwenhoven, D. van der Marel, C.T. Foxon, Phys. Rev. Lett. 60 (1988) 848.
[4] D.A. Wharam, T.J. Thornton, R. Newbury, M. Pepper, H. Ahmed, J.E.F. Frost, D.G. Hasko, D.C. Peacock, D.A. Ritchie, G.A.C. Jones, J. Phys. C 21 (1988) L209.
[5] L.I. Glazman, G.B. Lesovik, D.E. Khmelnitskii, R.I. Shekhter, Pis'ma Zh. Eksp. Teor. Fiz. 48 (1988) 329 [JETP Lett. 48 (1988) 238].
[6] L.I. Glazman, M. Jonson, Phys. Rev. B 41 (1990) 10 686.
[7] C.S. Chu, R.S. Sorbello, Phys. Rev. B 40 (1989) 5941.
[8] P. Bagwell, Phys. Rev. B 41 (1990) 10 354.
[9] J. Faist, P. Guéret, H. Rothuizen, Phys. Rev. B 42 (1990) 3217.
[10] F. Hekking, Y.V. Nazarov, Phys. Rev. B 44 (1991) 11 506.
[11] Q. Hu, Appl. Phys. Lett. 62 (1993) 837.
[12] R.A. Wyss, C.C. Eugster, J.A. del Alamo, Q. Hu, Appl. Phys. Lett. 63 (1993) 1522.
[13] R.A. Wyss, C.C. Eugster, J.A. del Alamo, Q. Hu, Appl. Phys. Lett. 66 (1995) 1144.
[14] Q. Hu, S. Verghese, R.A. Wyss, Th. Schäpers, J. del Alamo, S. Feng, Y. Yakubo, M.J. Rooks, M.R. Melloch, A. Förster, Semicond. Sci. Technol. 11 (1996) 1888.
[15] J.A. del Alamo, C.C. Eugster, Q. Hu, M.R. Melloch, M.J. Rooks, Superlatt. Microstruct. 23 (1998) 121.
[16] L. Fedichkin, V. Ryzhii, V. V'yurkov, J. Phys.: Condens. Matter 5 (1993) 6091.
[17] T.J.B.M. Janssen, J.C. Maan, J. Singleton, N.K. Patel, M. Pepper, J.E.F. Frost, D.A. Ritchie, G.A.C. Jones, J. Phys.: Condens. Matter 6 (1994) L163.
[18] L.Y. Gorelik, A. Grincwajg, V.Z. Kleiner, R.I. Shekhter, M. Jonson, Phys. Rev. Lett. 73 (1994) 2260.
[19] A. Grincwajg, L.Y. Gorelik, V.Z. Kleiner, R.I. Shekhter, Phys. Rev. B 52 (1995) 12 168.
[20] F.A. Maaø, L.Y. Gorelik, Phys. Rev. B 53 (1996) 15 885.
[21] C.S. Chu, C.S. Tang, Solid State Commun. 97 (1996) 119.
[22] Ola Tageman, L.Y. Gorelik, R.I. Shekter, M. Jonson, J. Appl. Phys. 81 (1996) 285.
[23] S. Feng, Q. Hu, Phys. Rev. B 48 (1993) 5354.
[24] C.S. Tang, C.S. Chu, Phys. Rev. B 60 (1999) 1830.
[25] P.F. Bagwell, R.K. Lake, Phys. Rev. B 46 (1992) 15 329.
[26] C.S. Tang, C.S. Chu, Phys. Rev. B 53 (1996) 4838.
[27] C.S. Tang, C.S. Chu, Physica B 254 (1998) 178.
[28] Y. Levinson, P. Wölfle, Phys. Rev. Lett. 83 (1999) 1399.
[29] M. Büttiker, Phys. Rev. Lett. 57 (1986) 1761.
[30] M. Büttiker, Phys. Rev. B 41 (1990) 7906.
[31] D.Y.K. Ko, J.C. Inkson, Phys. Rev. B 38 (1988) 9945.
[32] K. Yakubo, S. Feng, Q. Hu, Phys. Rev. B 54 (1996) 7987.
[33] P. Bhartia, I.J. Bahl, Millimeter Wave Engineering and Applications, Wiley, New York, 1984 (Chapter 3).